Elsevier Editorial System(tm) for Cement and Concrete Research

Manuscript Draft

Manuscript Number: CEMCON-D-15-00035R2

Title: Corrosion behavior of steel in alkali-activated fly ash mortars in the light of their microstructural, mechanical and chemical characterization

Article Type: Research Paper

Keywords: D. Alkali Activated Cement; C. Corrosion; D. Chloride; C. Mechanical Properties; B. Microstructure

Corresponding Author: Prof. Cecilia Monticelli, Prof.

Corresponding Author's Institution: University of Ferrara

First Author: Cecilia Monticelli, Prof.

Order of Authors: Cecilia Monticelli, Prof.; Maria E Natali, Ing.; Andrea Balbo, Dr.; Cristina Chiavari, Dr.; Federica Zanotto, Dr. Ing.; Stefania Manzi, Dr. Ing.; Maria C Bignozzi, Prof.

Abstract: This study concerns the corrosion behaviour of steel in different room temperature cured alkali-activated fly ash (FA) mortars exposed to chloride solution. The corrosion process was monitored by polarization resistance and corrosion potential measurements and the results were interpreted in the light of a complete microstructural, mechanical and chemical characterization of the mortars. The most compact alkali-activated mortars have higher porosity and lower mechanical properties than Ordinary Portland Cement mortar (CEM), but the protectiveness afforded to the rebars is slightly higher than that obtained in CEM. The reason for this discrepancy is connected to a lower chloride content accumulated in the former mortar type and to a specific inhibition of the rebar corrosion afforded by the pore electrolyte in alkali-activated mortars.

Ferrara 31 August 2015

To: Dr. Karen Scrivener, Editor-in-Chief of Cement and Concrete Research
Dr. Keith Baldie, Managing Editor of Cement and Concrete Research

Subject: submission of a reply to reviewer for the manuscript CEMCON-D-15-00035R1 to Cement and Concrete Research

Dear Editors,

We send you a reply to the comment of the reviewer, while we do not think to amend the manuscript CEMCON-D-15-00035R1:

" **Corrosion behavior of steel in alkali-activated fly ash mortars in the light of their microstructural, mechanical and chemical characterization**" by C. Monticelli, M.E. Natali, A. Balbo, C. Chiavari, F. Zanotto, S. Manzi, M.C. Bignozzi

Looking forward to your response

Best Regards,

Cecilia Monticelli

Prof. Cecilia Monticelli
Centro Studi Corrosione e Metallurgia "A. Daccò"
Dipartimento di Ingegneria - Università di Ferrara
Via Saragat, 1
44122 Ferrara
Tel 0039 0532 455136
Fax 0039 0532 455011
e-mail: mtc@unife.it
web: http://www.unife.it/centro/corrosione

**Response to Reviewers**

Reviewer #1: Does the Na2O/SiO2 ratio consist of SiO2 from the fly ash too? If so, the alkalinity is so high such that studying corrosion in such systems just becomes a topic of academic interest because of high alkalinity. Such systems cannot be practically handled also.

The Na2O/SiO2 ratios quoted in the manuscript take into consideration also the SiO2 content of the fly ash.
The ratio values used are in the range of those usually reported in the literature for geopolymers, as largely reported in the quoted references. Even if just the Na2O/SiO2 ratios of the activators are considered (0.66; 0.95; 1.32), the values fall inside the range usually reported and suitable to obtain a compact geopolymer microstructure.
As far as the handling of the investigated mixes is concerned, the same requirements usually adopted for concrete casting were used during the sample preparations of this work.
The mix can be easily handled just wearing a pair of laboratory gloves. The pH at the fresh state is comparable to that one exhibited by a fresh cement mix.
As further confirmation that geopolymer mortar/concrete can be handled with the same safety requirements usually adopted for concrete, we have also experienced the preparation of concrete blocks with large dimensions without meeting any particular danger.
Of course, special attention must be paid in preparing and handling the activating solutions.

# Corrosion behavior of steel in alkali-activated fly ash mortars in the light of their microstructural, mechanical and chemical characterization

C. Monticelli[a*], M.E. Natali[b], A. Balbo[c], C. Chiavari[d], F. Zanotto[e], S. Manzi[f] , M. C. Bignozzi[g]

[a*] *Corresponding author: Centro di Studi sulla Corrosione e Metallurgia "A. Daccò", Università di Ferrara, Via Saragat 1, 44122 Ferrara, Italy, tel. 0039 0532 455136, email: mtc@unife.it*

[b] *Dipartimento di Ingegneria Civile, Chimica, Ambientale e dei Materiali Università di Bologna, Via Terracini 28, 40131 Bologna, Italy, email: mariaelia.natali2@unibo.it*

[c] *Centro di Studi sulla Corrosione e Metallurgia "A. Daccò", Università di Ferrara, Via Saragat 1, 44122 Ferrara, Italy, email: andrea.balbo@unife.it*

[d] *CIRI-MAM Università di Bologna, Viale Risorgimento 2, 40136 Bologna (Italy), email: cristina.chiavari@unibo.it*

[e] *Terra&Acqua Tech, University of Ferrara, Via Saragat 1, 44122 Ferrara, Italy, email: federica.zanotto@unife.it*

[f] *Dipartimento di Ingegneria Civile, Chimica, Ambientale e dei Materiali Università di Bologna, Via Terracini 28, 40131 Bologna, Italy, email: stefania.manzi4@unibo.it*

[g] *Dipartimento di Ingegneria Civile, Chimica, Ambientale e dei Materiali Università di Bologna, Via Terracini 28, 40131 Bologna, Italy, email: maria.bignozzi@unibo.it*

**Keywords**

D. Alkali Activated Cement, C. Corrosion, D. Chloride, C. Mechanical Properties, B. Microstructure

**Abstract**

This study concerns the corrosion behaviour of steel in different room temperature cured alkali-activated fly ash mortars exposed to chloride solution. The corrosion process was monitored by polarization resistance and corrosion potential measurements and the results were interpreted in the light of a complete microstructural, mechanical and chemical characterization of the mortars. The most compact alkali-activated mortars have higher porosity and lower mechanical properties than a cement-based mortar (CEM), but the protectiveness afforded to the rebars is slightly higher than that obtained in CEM. The reason for this discrepancy is connected to a lower chloride content accumulated in the former mortar type and to a specific inhibition of the rebar corrosion afforded by the pore electrolyte in alkali-activated mortars.

## 1. Introduction

Reinforced concrete (RC) is the most commonly used construction material worldwide, but several problems can affect its matrix, in terms of durability and even sustainability.

As far as durability is concerned, the main factors that cause deterioration of RC are mostly linked to corrosion of the reinforcements, with consequent fatal decrease in terms of construction service life, loading capacities and seismic resistance, so that preventing corrosion is one of the most important goals to avoid RC deterioration. Normally, pH of the pore electrolyte in Ordinary Portland cement (OPC) is strongly alkaline (around 13 or even

higher), aiding the formation of a passive film which can prevent corrosion. This film can be damaged due to chloride attack [1-3] or due to carbonation, which causes a reduction of the pH of the pore electrolyte and undermines the stability of the passive film [4]. The binder plays a fundamental role in preventing or accelerating chloride penetration and concrete carbonation, because it affects the nature of the binder hydration products and the concrete porous microstructure.

Nowadays, worldwide commitments aim at achieving a more sustainable development by promoting a gradual replacement of Ordinary Portland Cement by binders with production systems at low-$CO_2$ emission [5]. In these terms, various studies have highlighted alkali-activated materials (AAM) as a potential competitive alternative to OPC [6,7]. This class of inorganic amorphous materials derives from the alkali-activation of aluminosilicate powders with suitable amorphous content. The final products have binding properties and engineering performances very similar to cement-based products and even superior in case of high temperature applications [8,9]. Many aluminosilicate precursors are suitable for activation and when the raw material has a high content of $SiO_2$+$Al_2O_3$ (generally >80%) and a low CaO content, like class F fly ash (FA), the final product is referred to as geopolymer [10]. The chance to use industrial by-products as precursors, such as FA or slags [11-13], along with a room or slightly higher curing temperature, makes AAM low-polluting products and, consequently, promising green building materials.

Many features of geopolymers obtained with different types of precursors have already been investigated, such as chemistry activation processes [14], gel-phase analysis [15], microstructure and mechanical properties [16,17]. As far as geopolymer durability is concerned, encouraging results have been obtained about their resistance to sulphate attack and alkali-silica reactions and about the high stability in the presence of fire or freeze-thaw cycles, beside an excellent adhesion to steel reinforcement [18]. Only a few studies focus on

room temperature (RT) activation [13,19,20], long-term performances and corrosion resistance of reinforcing bars in the presence of these alternative binding materials [18,21-25], which are key factors to permit the industrial application of these new mortar and/or concrete systems.

Early studies in this field show that, during 1-year exposure to a 95% R.H. atmosphere in the presence of 0 or 0.4% admixed chlorides, alkali activated FA mortar (cured at 85 °C) and a RT cured mortar with an alkali activated 70 FA/30 OPC binder mix afforded an excellent corrosion protection to the reinforcing bars. Protection was comparable to that obtained by traditional OPC mortar. On the contrary, with a 2% admixed chlorides, passive conditions were maintained for 200 days only in the mortar with the alkali-activated 70 FA/30 OPC binder mix, due to its lowest porosity [26]. After accelerated carbonation, FA mortars partially immersed in 0.2 M NaCl solutions afforded a higher corrosion protection to steel rebars than traditional mortar exposed to the same aggressive environment [27,28]. The reason was connected to the higher concentration of carbonate/bicarbonate ions in Na-containing pore electrolyte of FA mortars than in Ca-containing pore electrolyte of traditional OPC mortar. A high concentration of these ions is the consequence of the higher solubility of sodium carbonate/bicarbonate salts in comparison to calcium salts. Therefore, an effective pH buffer forms in carbonated FA mortars capable to hinder local pH variations induced by electrochemical activity of the rebars, connected to corrosion. This would hinder the formation of local galvanic cells and would inhibit corrosion [27].

Even the type of FA activator is expected to affect the corrosion behavior of reinforcing bars. In fact, the addition of sodium silicate to sodium hydroxide in the binder activating solution was found to induce lower porosity and higher mechanical properties in geopolymers [13,16,29-33]. As a consequence, an improvement of the corrosion resistance of the embedded rebars was measured [34].

The aim of this paper was to study the corrosion behavior of RT-cured steel-reinforced class F fly ash geopolymer mortars by an integrated approach based on mechanical, physical, microstructural and electrochemical tests. In particular, different formulations were prepared by changing the relative amounts of the activators in order to evaluate their effect on mechanical strength, porosity distribution and rebar corrosion behavior in a chloride-rich environment (NaCl 3.5 wt%). During the exposure, the chloride content in close proximity of the rebars and the initial and final pH values were also assessed. A comparison was made between geopolymer performances and those characterizing a cement-based mortar and the different behavior observed was justified on the basis of tests carried out in leachate solutions obtained from the different mortar types in contact with water.

## 2. Experimental

### *2.1. Raw materials*

Class F FA used as raw material for the geopolymer matrices was sourced from Enel Produzione S.p.A., Torrevaldaliga Nord power station (Civitavecchia, Roma, Italy), and was supplied by General Admixtures S.p.A. (Ponzano Veneto, Treviso, Italy). It exhibited a $d_{50}$=22 µm, while its mineralogical composition was found to have 65±0.8 wt% amorphous phase and crystalline phases of quartz, mullite and maghemite. The main oxide composition of FA is reported in Tab. 1. Detailed particle size distribution and mineralogical phase analysis are reported elsewhere [13]. Sodium silicate ($SiO_2/Na_2O$=1.99, density at 20 °C=1.5±0.2 g/cm$^3$, Ingessil, Verona, Italy) and 8 M NaOH were used as activating solutions and were mixed together and stirred 24 h before samples casting.

Reference mortar was prepared using CEM II/A-LL 42.5 R. For both geopolymer and cement-based mortars, natural calcareous sand ($d_{max}$=4 mm) was used as fine aggregate.

126 *2.2. Preparation of mortar specimens*

127 Three different geopolymer mortar mixes and a reference cement-based one were prepared.
128 Their mix design is shown in Tab. 2. All geopolymers were activated by adjusting the relative
129 amount of 8 M NaOH and sodium silicate solutions in order to achieve $Na_2O/SiO_2$ molar
130 ratios of 0.12, 0.14 and 0.16. The liquid/binder weight ratio (L/B) was fixed at 0.52.
131 The selected $Na_2O/SiO_2$ ratios were chosen on the basis of the results of a previous research
132 [13] where $Na_2O/SiO_2$ ratios ranging from 0.12 to 0.20 were investigated. Lower molar ratios
133 were not used as the determined loss of workability was found to critically affect mortar
134 samples preparation.
135 The geopolymer acronyms (FA12, FA14 and FA16) refer to the precursor name (FA) and the
136 $Na_2O/SiO_2$ molar ratio (e.g., FA16 indicates the FA-based mortar with a $Na_2O/SiO_2$ molar
137 ratio of 0.16). The reference mortar (CEM) was prepared with the same sand/binder and L/B
138 ratios adopted for geopolymer mortars (Tab. 2).
139 Microstructural and mechanical characterizations were performed on prismatic samples
140 (40x40x160 $mm^3$), mechanically compacted and de-molded after 1 day curing at T=25 °C and
141 R.H.=35%. Then, the specimens were kept at the laboratory atmosphere (R.H.≈35%) and tests
142 were performed in due time. These exposure conditions aim at reproducing those often
143 adopted at the construction sites.
144 Electrochemical tests and analyses of penetrated chloride content were carried out on slabs
145 with dimensions 200x250x50 $mm^3$. Three manually compacted slabs were prepared for each
146 formulation: two reinforced slabs with embedded steel bars (Fig. 1a) and one unreinforced
147 slab for chloride concentration analysis (Fig. 1b). Each reinforced slab contained two
148 sandblasted degreased ribbed carbon steel rods acting as working electrodes (W, φ=10 mm),
149 with ends masked with epoxy resin and isolated by thermo-shrinking adhesive tape to leave
150 an exposed surface area of 7400 $mm^2$. In close proximity to these bars, two activated titanium

wires and three symmetrically arranged stainless steel bars acted as reference (R) and counter (C) electrodes, respectively, during the electrochemical tests.

Slabs were cured in the molds at T=25 °C and R.H.=35% for a week, then they were de-molded and cured at the laboratory atmosphere (R.H.≈35%) for further 3 weeks, again to simulate practices often adopted in field applications. Finally, the lower side of each slab was ground so reducing the slab thickness by 2 mm, in order to avoid the skin effect and accelerate the ingress of chlorides. The ground side was finally exposed to the aqueous chloride solution, without slab pre-saturation (Fig. 2).

### *2.3. Characterization*

#### *2.3.1. Microstructure and mechanical characterization*

Compressive strength ($\sigma_c$) was measured by an Amsler-Wolpert machine (maximum load: 100 kN) at a constant displacement rate of 50 mm/min. The results are reported as average values of 5 measurements, respectively. Flexural strength measurements were also carried out and the results are reported in [25].

Two different tests were performed to determine water absorption properties by capillarity. The first test was accomplished with a procedure similar to the one described in UNI EN 1015-18 [35] on prismatic samples after flexural test. The capillary coefficient was determined according to the formula $C=0.1\cdot(W_2-W_1)$ kg/m$^2\cdot$min$^{0.5}$ and the height of water capillary penetration was measured at the end of the test by longitudinally splitting the samples. The second test was performed according to UNI EN 15801 [36]: the weight gain of pre-dried regular form samples, partially immersed in a constant 5 mm water head, was monitored over 8 days. The amount of water absorbed per unit area was plotted as a function of $\sqrt{t}$ for the determination of the capillary absorption curve.

Pore size distribution measurements were carried out on mortar samples of about 1 $cm^3$. The tests were carried out by a mercury intrusion porosimetry (MIP) (Carlo Erba 2000) equipped by a macropore unit (Model 120, Fison Instruments). A mercury surface tension of 0.48 N/m and a contact angle of 141.3° were assumed [37].

*2.3.2. Tests under partial immersion conditions*

After 28 days of curing, reinforced and unreinforced slabs were exposed without any water pre-saturation to a 3.5% NaCl solution for 90 days with a constant water head of 1 mm. A controlled dripping device with an associated spillway ensured this level (Fig. 2). Two reinforced and one unreinforced slab for each mortar type were tested. The adopted exposure condition is particularly severe because it produces capillary suction of the aggressive solution and continuous evaporation from the upper slab surface in contact with the low R.H. atmosphere of the lab (R.H.≈35%). Consequently, salt concentration and crystallization inside the mortar in regions close to the upper evaporation surface occurs, as already described by other authors [38].

In order to avoid significant variations of the concentration of the chloride solution in contact with the slabs, the solution was renewed each month.

Electrochemical tests were performed by a 273A PAR instrument and consisted in corrosion potential ($E_{cor}$) and polarization resistance ($R_p$) measurements, always carried out on all the embedded rebars (4 repetitions). Before each potentiostatic test, $E_{cor}$ was measured both versus the inner Ti quasi-reference electrode and versus an external saturated calomel electrode (SCE), applied on the mortar surface in correspondence of the rebar. An interlaying wet pad minimized the ohmic drop.

The polarization resistance values were obtained by a potentiostatic method, that is by applying an anodic 20 mV potentiostatic step lasting 300 s and by measuring the obtained

final constant anodic current. Corrections for ohmic drop were not necessary because, as assessed by preliminary EIS (Electrochemical Impedance Spectroscopy) tests, the ohmic drop between the working and quasi-reference electrodes was always negligible with respect to the obtained $R_p$ values.

In order to evidence the tendency to carbonation under partial immersion conditions, at the end of the exposure to 3.5% NaCl solution the reinforced slabs were longitudinally sectioned and the pH value of the pore electrolyte in the mortar portions close to the rebars was measured by a leaching method. In particular, 5 g ground mortar samples were mixed with 5 $cm^3$ distilled water, at room temperature. The pH of the obtained leachate solution was deemed an acceptable approximation of the pH of the mortar pore electrolyte [27,39].

On unreinforced slabs exposed to 3.5% NaCl solution, the distribution of total chloride content was evaluated on core drills (φ=2 cm, h=5 cm, Fig. 1b), extracted at specific time intervals (10, 30, 60 and 90 days). In order to maintain unaltered the chloride transport into the slabs, after core extraction an epoxy varnish sealed the surfaces of the holes left in the slabs. The cores were transversally cut in 5 slices (φ=20 mm, h=7 mm) and the $4^{th}$ slice, characterized by the same distance from the solution level as that of the rebars in reinforced slabs, was powdered (5 g) and analyzed for total chloride content by potentiometric titration, according to ASTM C1152/C1152M [40] and ASTM C114 [41]. Therein, the chloride contents were considered equal to those in the mortar regions surrounding the reinforcing bars.

*2.3.3. Rebar surface analyses*

After the electrochemical tests, cross-sections of the rebars in reinforced slabs were obtained and analyzed through Optical Microscopy (OM) Zeiss and a Variable Pressure Scanning Electron Microscope (VP-SEM) Zeiss EP EVO 50 with secondary and back scattered

electrons detectors. The images from VP-SEM were collected in Variable Pressure mode (80Pa). The accelerating voltage used for analyses was 20 keV. At the end of the exposures to 3.5% NaCl solution the corrosion products formed on the rebars embedded in reinforced slabs were analyzed through Raman measurements by a Renishaw Raman Invia instrument. The experimental conditions were defined as following and checked in order to avoid thermal degradation of iron corrosion products: the laser was a Ar+ laser (514.5nm), the integration time (t) was 10 s, the number of accumulations (n) was 4 and the laser power (Pout) was 3 mW).

*2.3.4. Tests in leachate solutions*

In an attempt to investigate more deeply the corrosion behavior of the rebars in the different mortars, one prismatic specimen (about 500 g) of each mortar type was finely ground after 28 days curing and mixed with water according to a 1:0.5 ratio, to extract the soluble species present in the pore electrolyte. After 2 min stirring, the leachate solution was filtered and its elemental analysis was accomplished by Inductively Coupled Plasma-Optical Emission Spectroscopy (ICP-OES, Serie Optima 3200 XL, Perkin Elmer). Finally, the solution was used as electrolyte in a three-electrode cell for recording the polarization curves on steel. With this aim, flat steel electrodes with an exposed area of about 80 $mm^2$ were prepared from the corrugated bars. They were ground and polished by 1 µm diamond paste. After 1 h immersion, polarization curves were recorded, at a potential scan rate of 0.167 mV/s. Cathodic and anodic polarization curves were recorded on different electrodes starting from $E_{cor}$. Tests were performed in duplicate. All the potentials are referred to SCE.

## 3. Results and discussion

*3.1. Microstructure and mechanical characterization*

Geopolymer and cement mortars showed similar values of bulk density (i.e., 2.04±0.01 g/cm$^3$ for geopolymers and 2.07±0.01 g/cm$^3$ for CEM).

The compressive strength values of the investigated mortars at different curing times are reported in Fig. 3. Fig. 3a shows that the compressive strength values of geopolymers increased with curing time for up to 28 days of curing, as occurs in traditional mortars. As a consequence, 28 days can be considered as a representative curing time for estimating geopolymer strength, similarly to cement standard compressive strength determined according to EN 196-1 [42]. After 28 days, the compressive strength values ($\sigma_{c28}$) increased for geopolymers following this order: $\sigma_{c28}$FA16<$\sigma_{c28}$FA14<$\sigma_{c28}$FA12 (i.e., 17.2±0.9<18.9±0.6<23.3±0.3 MPa) and were similar to those obtained by other authors on similar materials cured at room temperature or by mild heating [19,20].

At decreasing $Na_2O/SiO_2$ molar ratio, compressive strength increased linearly (Fig. 3b). The increase of $\sigma_c$ values at higher silicate contents was more evident at early curing time, suggesting that a high silicate concentration stimulated the rate of geopolymerization [29]. The effect of sodium silicate in promoting the geopolymeric net formation and in reducing the total porosity (at least in specific $Na_2O/SiO_2$ ranges) is also elsewhere highlighted [13,16,29,30]. In particular, in a research carried out on geopolymers with a constant Na/Al ratio, an increase in Si/Al (and therefore Si/Na) ratio induced an increase in gel volume, homogeneity and strength and, likely, also an increase in the intrinsic binder strength, because the stronger Si-O-Si linkages substituted the weaker Si-O-Al and Al-O-Al bonds [33]. Conversely, a too high Si/Al ratio produced a high unreacted phase fraction and induced a decrease of mechanical performances [33]. CEM exhibited a compressive strength of 34.4±0.5 MPa at 28 days of curing (Fig. 3a), which was higher than that of geopolymers. This value, quite low for a CEM 42.5 R, was due to factors such as the relatively high L/B ratio, the use of non-standard sand and curing conditions (R.H.=35%).

The sample microstructure was investigated by means of water absorption and MIP measurements. After 90 min (short test), the absorbed water reached penetration heights of about 45 mm in all geopolymers, while a lower height of 25 mm was measured for CEM. The capillary water absorption coefficients, reported in Fig. 4a, were quite similar for all geopolymers (with a maximum value of 0.43 $kg/m^2 \cdot min^{0.5}$ for FA16), while a lower value was registered for CEM (0.36 $kg/m^2 \cdot min^{0.5}$). These results suggest that the latter mortar has a refined and perhaps more tortuous pore structure than that of FA mortars [43].

In spite of the slow water uptake rate detected on CEM at short exposure times, the longer lasting water absorption tests (Fig. 4b) evidenced that the final water uptake of CEM was comparable or even higher than that exhibited by geopolymers ($Q_i$=7.2 $kg/m^2$ in CEM and $Q_i$=6.7 $kg/m^2$ in FA16). In fact, after 8 days the water uptake of CEM was twice that obtained after 90 min, while that achieved by geopolymers did not increase much. These data indicated that in both mortar types a significant water absorption occurred, which was faster in geopolymer materials.

The pore size distributions of all mortars were assessed by MIP analysis after 28 days of curing and the results are reported in Fig. 5a. In this plot, three different pore size regions can be distinguished: gel pores below 0.015 μm (which do not affect permeability [44]), capillary pores ranging between 0.015-0.5 μm (affecting fluid permeability and mechanical properties [45,46]) and macropores with radius ≥ 0.5 μm, mainly influencing mechanical properties [47]. The Figure shows that the main observable difference between geopolymer and cement-based mortars was the large presence of macropores in geopolymers and the predominance of capillary pores in CEM. Among geopolymers, FA16 exhibited the most porous microstructure, while similar pore size distributions were observed for FA12 and FA14. Other important information can be drawn by the comparison of the $r_{50\%}$ values, which are the pore radii at which 50% of the pore volume is intruded in the different matrices. Fig. 5b reports the

normalized pore size distributions for all the investigated mortar types and shows that the $r_{50\%}$ of CEM mortar was 0.19 µm, much lower than that obtained for geopolymers (around 1 µm for all mixes), in agreement with the slower observed water uptake detected during absorption tests in CEM mortar. Among geopolymers, a slightly higher $r_{50\%}$ value was found in FA16 (i.e., FA12=1.23 µm; FA14=1.27 µm and FA16=1.36 µm).), suggesting that this mortar is more vulnerable to the penetration of aggressive species from aqueous solutions.

*3.3. Tests under partial immersion conditions*

During the 90 day exposure to 3.5% NaCl solution, chlorides penetrated through the mortars by a combination of capillary suction and diffusion. Capillary suction is the fastest process and, on the basis of absorption tests, the chloride solution is expected to reach the reinforcing bars (at a height of 33 mm, Fig. 2) in less than 1 day in all mortars.

Fig. 6 shows the average $E_{cor}$ (Fig. 6a) and $R_p$ (Fig.6b) trends obtained in all mortars, while the shadowed regions define the interval $E_{cor}\pm\sigma_E$ ($E_{cor}$ standard deviation) and $R_p\pm\sigma_R$ ($R_p$ standard deviation). Within 2 days of exposure, the average $E_{cor}$ values of rebars in CEM underwent a fast drop from about -0.1 $V_{SCE}$ down to values more negative than -0.276 $V_{SCE}$ (Fig. 6a) that is the limit that, according to ASTM C876 [48], indicated a high probability of active corrosion. The same occurred within about 6 days of exposure in FA12 and FA14 and after only 1 day in FA16 mortars. Later, values around -0.55 $V_{SCE}$ on average were obtained in CEM and even more negative in FA12 and FA14 and particularly in FA16 (on average -0.60÷-0.65 $V_{SCE}$, Fig. 6a).

On the basis of a generally accepted Stern and Geary constant of 26 mV, the $i_{cor}$ limit for active corrosion ($i_{cor}$ of $0.2\cdot10^{-6}$ A $cm^{-2}$, according to [49]) is reached in correspondence of a $R_p$ value of $1.3\cdot10^5$ ohm·$cm^2$. Fig. 6b shows that the average $R_p$ values of the rebars decreased from initial values close to $3\cdot10^6$ ohm·$cm^2$ to values lower than about $10^5$ ohm·$cm^2$ within 1-2

days of exposure in CEM and FA16 and after about 40 days, in the case of FA12 and FA14. At the end of the exposure period, low and comparable average $R_p$ values ($3 \cdot 10^4 \div 4 \cdot 10^4$ ohm·cm$^2$) were recorded in all mortar types.

These findings suggested that a corrosion attack developed in all mortars, but a less severe one occurred in FA12 and FA14 formulations. These mortars exhibited a lower porosity than FA16 (Fig. 5a), so justifying their better protectiveness towards the rebars. However, their cumulative porosity was similar to that of CEM, which was characterized by finer pores. So the worse behavior of CEM towards degradation was unexpected.

In order to elucidate this apparent inconsistency, further tests were performed, starting with the measurement of the pH and the chloride content of the pore electrolytes in contact with the rebars.

The pH values of the mortar pore electrolyte at the rebar level were measured at the end of the 90 day exposure to the NaCl solution. In Tab. 3, these pH values are compared to the initial values, measured after 1 day curing. A negligible pH decrease was detected in CEM and a pH reduction of about 0.5 pH unit was found in FA mortars. Anyway, all pH values remained higher than 12, suggesting that significant carbonation was not experienced and did not affect the corrosion behavior.

The total Cl- content (% *vs* binder) again at the rebar level in the different mortars was determined after different exposure times (Fig. 7). In all mortars, the chloride amounts increased for up to 60 days and then remained more or less constant until the end of the test. Higher chloride contents were detected in CEM (5% *vs* binder at the end of the test) than in geopolymers (1.4-1.8% *vs* binder at the end of the test). This was caused by the lower solubility of calcium-containing chloride salts formed in CEM (e.g., Friedel salts), in comparison to the sodium-containing chloride salts present in FA mortars. In the latter case, the salts were leached away by the contact solution, ensuring the maintenance of a lower

chloride concentration. Chloride concentrations in AAMs similar to those reported in Fig. 7 were achieved after 7 days of exposure to saturated NaCl solution by [50]. Moreover, analyses carried out after 300 days of full or partial immersion of traditional mortar (obtained with water/cement ratio of 0.65 and moist curing) in 3.5% NaCl solution revealed chloride concentrations (expressed as of mass fraction of chloride ions in cement mortar) close to those here reported in CEM at saturation [38]. In that research, the authors stressed that during partial immersion exposures much higher chloride amounts penetrated inside the mortars with respect to full immersion conditions because of the concomitant effect of continuous capillary penetration and water evaporation [38].

After only 10 days of exposure in 3.5% NaCl solution, the $Cl^-$ content in CEM and FA mortars was quite high: about 0.7 and 0.5% *vs* binder, respectively. The achieved chloride concentrations are higher than the commonly accepted critical chloride content capable to initiate corrosion in traditional concrete [1] and were actually found to be sufficient to start corrosion in CEM and FA16. On the contrary, a significant corrosion rate in FA12 and FA14 was measured only after 40-50 days when the chloride content was in the range 1-1.7 % *vs* binder. A higher critical content is likely to characterize the more compact geopolymers. The reason for this different behavior was unclear and was elucidated by recording polarization curves on steel in leachate solutions (paragraph 3.5).

### 3.4. *Rebar surface analyses*

Fig. 8a shows the surface aspect of the rebars after the partial immersion in chloride solution. In agreement with the active $E_{cor}$ values and relatively low $R_p$ measured by the electrochemical tests, significant corrosion attacks were detected in all rebars. In particular, a significant localized corrosion attack was present in CEM mortar, with pit depths around 300 µm (Fig. 8b), while a widespread general non-uniform corrosion attack occurred in FA

mortars and particularly in FA16. As an example, Fig. 9 reports a SEM image showing a uniform corrosion layer (200-400 µm thick), which covered part of the reinforcing bar in FA16 (as shown in Fig. 8a).

The Raman analysis of the corrosion products formed in the different mortar types (Tab. 4) revealed the presence of Maghemite ($\gamma$-$Fe_2O_3$) and $\delta$-FeOOH in all samples, while Akaganeite ($\beta$-FeOOH) was found only in the geopolymer matrices. This latter corrosion product, usually connected to chloride-contaminated environments [51], is characterized by a low protectiveness and justifies the occurrence of a general corrosion attack in geopolymer mortars, instead of a localized attack, as detected in CEM.

### 3.5. *Tests in leachate solutions*

Fig. 10 collects the polarization curves recorded in the leachate solutions obtained from the different mortars. It clearly shows that in all cases steel exhibits a passive behavior at $E_{cor}$, which is close to -0.38 $V_{SCE}$, independently of the mortar type. Passivity persists up to a potential of about 0.6-0.7 $V_{SCE}$, where oxygen evolution occurs [52] and it is slightly stronger in solutions obtained from geopolymers. In fact, passive currents are smaller than in solutions extracted from CEM. Also cathodic polarization curves recorded in geopolymer leachate solutions are shifted to lower currents. Consequently, $i_{cor}$ values in solutions extracted from geopolymers are about one half of that obtained in CEM extracts ($2.4 \cdot 10^{-8}$ A $cm^{-2}$ towards $5.1 \cdot 10^{-8}$ A $cm^{-2}$ on average).

This means that, in spite of the presence of a pH value slightly lower than that detected in CEM, a corrosion inhibitor is present in the FA mortar pores electrolyte, which hinders steel corrosion.

ICP-OES analyses reported in Tab. 5 show that leachate solutions deriving from FA mortars differ from those extracted from CEM essentially for the presence of relevant amounts of

silicates in the former case ([Si]=0.02-0.03 M in FA mortars, absent in CEM). Silicates are known to be corrosion inhibitors for iron and steel [53,54] and are reputed the origin of the observed slightly better corrosion behavior of steel in geopolymers.

## 4. Conclusions

In this work reinforced and unreinforced FA-based mortar samples were prepared at RT with a constant L/B ratio of 0.52 and decreasing $Na_2O/SiO_2$ ratios in the activating solutions. Their microstructure and mechanical behavior, along with their corrosion and chloride penetration resistance, were analyzed and compared to those exhibited by a cement-based mortar with the same L/B ratio. The multiple characterization techniques used in this work permitted to draw the following conclusions:

- The mechanical properties of FA mortars were found to be inversely proportional to the $Na_2O/SiO_2$ molar ratio. In particular, a high silicate content appears to stimulate the rate of geopolymerization and densification. All geopolymers showed higher porosity and lower mechanical performances than CEM mortar;
- During exposure to NaCl solution, no carbonation was detected at the rebar level. Chloride concentrations were higher in CEM than in geopolymers, due to the formation of scarcely soluble calcium-containing chloride salts;
- Electrochemical tests showed that the most compact geopolymers (FA12 and FA14) were more protective than FA16 and CEM towards steel rebars. The lower chloride contents generally present in geopolymers with respect to CEM can help to justify these differences. The lower protectiveness of FA16 was due to its higher porosity;
- FA12 and FA14 showed a higher critical chloride content for corrosion onset (about 1-1.7% *vs* binder), than CEM (around 0.5%). The better performance of these denser geopolymers

was connected to the presence of soluble silicate ions in geopolymer pore electrolytes which exerted a specific inhibition of rebar corrosion;

• At the end of the partial immersion test, a corrosion attack started on all rebars, independently of the mortar type. In geopolymers, the surface film contained akaganeite , which induced a general non-uniform corrosion attack. In CEM, different surface conditions occurred which caused the localization of the attack in deep pits.

**Acknowledgements**

The authors wish to thank Dr. L. Carabba for her useful assistance in sample preparation and microstructural and mechanical characterizations and Dr. M. Abbottoni for his valuable assistance in performing part of the electrochemical measurements and chloride analysis.

**References**

[1] U. Angst, B. Elsener, C.K. Larsen, G.C. Luckey, Ø Vennesland, Critical chloride content in reinforced concrete – A review, Cement Concrete Res. 39 (2009) 1122-1138.

[2] A. Neville, Chloride attack of reinfonced concrete: an overview, Mater. Struct. 28 (1995) 63-70.

[3] I. Ustabas, The effect of capillarity on chloride transport and prediction of the accumulation region of chloride in concretes with reinforcement corrosion, Constr. Build. Mater. 28 (2012) 640-647.

[4] F. Pacheco-Torgal, S. Miraldo, J.A. Labrincha, J. De Brito, An overview on concrete carbonation in the context of eco-efficient construction: Evaluation, use of SCMs and/or RAC, Constr. Build. Mater. 36 (2012) 141-150.

[5] M. Uwasua, K. Haraa, H. Yabar, World cement production and environmental implications, Environ. Dev. 10 (2014) 36-47.

449 [6] P. Duxson, A. Fernández-Jiménez, J.L. Provis, G.C. Luckey, A. Palomo, J.S.J van
450 Deventer, Geopolymer technology: the current state of the art, J. Mater. Sci. 42 (2007) 2917-
451 2933.
452 [7] P. Duxson, J.L. Provis, G.C. Luckey, J.S.J. van Deventer, The role of inorganic polymer
453 technology in the development of 'Green Concrete', Cement Concrete Res. 37 (2007) 1590-
454 1597.
455 [8] T. Bakharev, Thermal behavior of geopolymers prepared using class F fly ash and
456 elevated temperature curing, Cement Concrete Res. 36 (2006) 1134-1147.
457 [9] W.D.A. Rickard, J. Temuujin, A. van Riessen, Thermal analysis of geopolymer pastes
458 synthesised from five fly ashes of variable composition, J. Non-Crys. Solids 358 (2012)1830-
459 1839.
460 [10] J. Davidovits, Geopolymer: inorganic polymeric new materials, J. Therm. An. 37 (1991)
461 1633-1656.
462 [11] M. C. Bignozzi, S. Manzi, I. Lancellotti, E. Kamseu, L. Barbieri, C. Leonelli, Mix-design
463 and characterization of alkali activated materials based on metakaolin and ladle slag, Appl.
464 Clay Sci. 73, (2013) 78-85.
465 [12] M. Komjenovic, Z. Bascarevic, V. Bradic, Mechanical and microstructural properties of
466 alkali-activated fly ash geopolymers, J. Hazard. Mater. 181 (2010) 35-42.
467 [13] M.C. Bignozzi, S. Manzi, M.E. Natali, W.D.A. Richard, A. van Riessen, Room
468 temperature alkali activation of fly-ash: the effect of $Na_2O/SiO_2$ ratio, Constr. Build. Mater.
469 69 (2014) 262-270.
470 [14] A. Fernández-Jiménez, A. Palomo, Composition and microstructure of alkali activated
471 fly ash binder: Effect of the activator, Cem. Concr. Res. 35 (2005) 1984-1992.

[15] F. Winnefeld, A. Leemann, M. Lucuk, P. Svoboda, M. Neuroth, Assessment of phase formation in alkali activated low and high calcium fly ashes in building materials, Constr. Build. Mater. 24 (2010) 1086-1093.

[16] G.S. Ryu, Y.B. Lee, K.T. Koh, Y.S. Chung, The mechanical properties of fly ash based geopolymer concrete with alkaline activators, Constr. Build. Mater. 47 (2013) 409-418.

[17] P. Sukmak, S. Horpibulsuk, S.L. Shen, Strength development in clay-fly ash geopolymer, Constr. Build. Mater. 40 (2013) 566-574.

[18] F. Pacheco-Torgal, Z. Abdollahnejad, A.F. Caomoes, M. Jamshidi, Y. Ding, Durability of alkali-activated binders: A clear advantage over Portland cement or an unproven issue?, Constr. Build. Mater. 30 (2012) 400-405.

[19] N.K. Lee, H.K. Lee. Setting and mechanical properties of alkali-activated fly ash/slag concrete manufactured at room temperature, Constr. Build. Mater. 47 (2013) 1201-1209.

[20] I. Ismail, S.A. Bernal, J.L. Provis, R. San Nicolas, D.G. Brice, A.R. Kilcullen, et al, Influence of fly ash on the water and chloride permeability of alkali activated slag mortars and concrete, Constr. Build. Mater. 48 (2013) 1187-1201.

[21] P. Chindaparasirt, W. Chalee, Effect of sodium hydroxide concentration on chloride penetration and steel corrosion of fly ash-based geopolymer concrete under marine site, Constr. Build. Mater. 63 (2014) 313-310.

[22] M.d.S. Badar, K. Kupwade-Patil, S.A. Bernal, J.L. Provis, E.N. Allouche, Corrosion of steel bars induced by accelerated carbonation in low and high calcium fly ash geopolymer concretes, Constr. Build. Mater. 61 (2014) 79-89.

[23] C. Monticelli, M. Abbottoni, S. Manzi, C. Chiavari, A. Balbo, F. Zanotto, M.E. Natali, M.C. Bignozzi, Corrosion behavior of steel in fly-ash geopolymer mortars exposed to chloride solutions, Eurocorr 2014; Paper n. 7261.

[24] C. Monticelli, M. Abbottoni, S. Manzi, C. Chiavari, A. Balbo, F. Zanotto, M.E. Natali, M.C. Bignozzi, Investigations of chloride diffusion for reinforced geopolymer mortar, Eurocorr 2014; Paper n. 7551.

[25] M.E. Natali, S. Manzi, L. Carabba, C. Chiavari, M.C. Bignozzi, M. Abbottoni, A. Balbo, C. Monticelli, Mechanical performances and corrosion resistance of reinforced fly ash mortars,. Advances in Sci. and Technol. 92 (2014) 50-55.

[26] D.M. Bastidas, A. Fernández-Jiménez, A. Palomo, J.A: González, A study on the passive state stability of steel embedded in activated fly ash mortars, Corr. Sci. 50 (2008) 1058-1065.

[27] C. Monticelli, M. Criado, S. Fajardo, J.M. Bastidas, M. Abbottoni, A. Balbo, Corrosion behavior of a low Ni austenitic stainless steel in carbonated chloride-polluted alkali-activated fly ash mortars, Cem. Concr. Res. 55 (2014) 49-58.

[28] M. Criado, C. Monticelli, S. Fajardo, D. Gelli, V. Grassi, J.M. Bastidas, Organic corrosion inhibitor mixtures for reinforcing steel embedded in carbonated alkali-activated FA mortar, Constr. Build. Mater. 35 (2012) 30-37.

[29] H.K. Tchakoute, A. Elimbi, E. Yanne, C.N. Djangang, Utilization of volcanic ashes for the production of geopolymers cured at ambient temperature, Cem. Concr. Comp. 38 (2013) 75-81.

[30] M. Criado, A. Fernández-Jiménez, A.G. de la Torre, M.A.G. Aranda, A. Palomo, An XRD sudy of the effect of the $SiO_2/Na_2O$ ratio on the alkali activation of fly ash, Cem. Concr. Res. 37 (2007) 671-679.

[31] J.M. Miranda, A. Fernández-Jiménez, J.A. González, A. Palomo, Corrosion resistance in activated fly ash mortars, Cem. Concr. Res. 35 (2005) 1210-1217.

[32] M. Criado, S. Martínez-Ramirez, S. Fajardo, P.P. Gómez, J.M. Bastidas, Corrosion rate and corrosion product characterisation using Raman spectroscopy for steel embedded in chloride polluted fly ash mortar, Mater. Corr. 64 (2013) 372-380.

521 [33] P. Duxson, J.L. Provis, G.C. Lukey, S.W. Mallicoat, W.M. Kriven, J.S.J. van Deventer,
522 Understanding the relationship between geopolymer composition, microstructure and
523 mechanical properties, Colloids Surf. A: Physicochem. Eng. Aspects. 269 (2005) 47-58.
524 [34] A. Fernández-Jiménez, J.M. Miranda, J.A. González, A. Palomo, Steel passive state
525 stability in activated fly ash mortars, Mater. Construc. 60, 300 (2010) 51-65.
526 [35] UNI EN 1015-18. Methods of test for mortar for masonry – determination of water
527 absorption coefficient due to capillary action of hardened mortar. 2002.
528 [36] UNI EN 15801. Conservation of cultural property-Test methods-Determination of water
529 absorption by capillarity. 2010.
530 [37] DIN 66133. Determination of pore volume distribution and specific surface area of solids
531 by mercury intrusion. 1993.
532 [38] K-L. Ma, Y-J. Xie, G-G. Long, K-G. Wu, Invading track of chloride ions in cemented-
533 based materials, J. Cent. South Univ. Technol. 17 (2010) 263-268.
534 [39] V. Räsänen, V. Penttala, The pH measurement of concrete and smoothing mortar using a
535 concrete powder suspension, Cem. Concr. Res. 34 (2004) 813-820.
536 [40] ASTM C1152/C1152M. Standard test method for acid-soluble chloride in mortar and
537 concrete. 2004.
538 [41] ASTM C114. Standard test methods for chemical analysis of hydraulic cement. 2011.
539 [42] EN 196-1. Methods of testing cement – Part 1: determination of strength. 2005.
540 [43] H. Zhu, Z. Zhang, Y. Zhu, L. Tian, Durability of alkali-activated fly ash concrete:
541 Chloride penetration in pastes and mortars, Construction and Building Materials 65 (2014)
542 51-59.
543 [44] P.K. Metha, D. Manmohan, Pore size distribution and permeability of hardened cement
544 paste. 7th International Symposium of the Chemestry of Cement, Paris,1980, pp. 1-5.

[45] Rilem report 12. In: Kropp J, Hilsdorf HK, editors. Performance criteria for concrete durability. 1995.

[46] R. Kumar, B. Bhattacharjee, Porosity, pore size distribution and in situ strength of concrete, Cem. Concr. Res. 33 (2003) 155-164.

[47] J.X. Zhang, T. Fujiwara, Resistance to frost damage of concrete with various mix proportions under salty condition, frost resistance of concrete, RILEM proceedings PRO. Cachan Cedex, France: RILEM Publications Carl, 2002, pp. 367-74.

[48] ASTM C876. Standard test method for half-cell potentials of uncoated reinforcing steel in concrete. 2009.

[49] C. Andrade, M.C. Alonso, J.A. González, An initial effort to use the corrosion rate measurements for estimation rebar durability, in: Berke NS, Chaker V, Whiting D. (eds.). Corrosion rates of steel in concrete ASTM STP 1065, American Society for Testing and Materials, Philadelphia, 1990, pp. 29-37.

[50] H. Zhu, Z. Zhang, Y. Zhu, L. Tian, Durability of alkali-activated fly ash concrete: Chloride penetration in pastes and mortars, Constr. Build. Mater. 65 (2014) 51-59.

[51] P. Refait, J.M.R. Genin, The mechanisms of oxidation of ferrous hydroxychloride β-$Fe_2(OH)_3Cl$ in aqueous solution: The formation of akaganeite *vs* goethite, Corros. Sci. 33 (1993) 539-553.

[52] E. Volpi, A. Olietti, M. Stefanoni, S.P. Trasatti, Electrochemical characterization of mild steel in alkaline solutions simulating concrete environment, J. Electroanal. Chem. 736 (2015) 38-46.

[53] S.T. Amaral, I.L. Müller, Passivation of pure iron in alkaline solution containing silicate and sulphate-galvanostatic and potentiostatic studies, Corros. Sci. 41 (1999) 747-758.

[54] S.T. Amaral, I.L. Müller, A RRDE study of the electrochemical behavior of iron in solutions containing silicate and sulphate at pH 10–13, Corros. Sci. 41 (1999) 759-771.

571

572 **Figure Captions**

573 **Figure 1.** Geometric scheme of the slabs (dimensions are expressed in mm): a) reinforced
574 slab: W= working electrodes, C=stainless steel counter electrodes, R=activated Ti reference
575 electrodes; b) unreinforced slab: core drills for $Cl^-$ analysis are highlighted in dashed line

576

577 **Figure 2.** Geometric section of the reinforced slab and set-up for tests under partial
578 immersion conditions (dimensions in mm). The 3.5% NaCl solution head in contact with the
579 specimen is 1 mm high

580

581 **Figure 3.** a) Compressive strength values ($\sigma_c$) of the investigated mortar samples at different
582 curing times (2, 7, 28, 60 and 90 days); b) Compressive strength values ($\sigma_c$) of geopolymer
583 mortars at different times of curing (7, 28 and 90 days) as a function of the $Na_2O/SiO_2$ molar
584 ratio

585

586 **Figure 4.** a) Capillary water absorption coefficients according to UNI EN 1015-18 [35]; b)
587 Amount of water absorbed per unit area according to UNI EN 15801 [36]

588

589 **Figure 5.** a) Pore size distribution curves of the investigated samples at 28 days of curing; b)
590 Normalized pore size distribution curves of the investigated samples at 28 days of curing.
591 Mean pore radius values ($r_{50\%}$) are highlighted by dashed lines

592

593 **Figure 6.** Average $E_{cor}$ (a) and $R_p$ (b) values recorded in the different mortar types during
594 partial immersion in 3.5% NaCl solution. The hatched regions evidence the variability of $R_p$
595 and $E_{cor}$ values (average±standard deviation) within rebars embedded in the same mortar type.

For the sake of simplicity, the variability region for FA14 is omitted, because it more or less overlaps that of FA12

**Figure 7.** Total $Cl^-$ content (% *vs* binder) at the rebar section for the investigated samples

**Figure 8.** a) Reinforcing bars extracted from the slab at the end of the corrosion tests; b) Cross-section optical micrograph of rebar in reinforced CEM slab at the end of the corrosion tests

**Figure 9.** Cross-section SEM micrograph of rebar in reinforced FA16 slab at the end of the corrosion tests

**Figure 10.** Polarization curves recorded in the leachate solutions obtained from the different mortar types

611

612 Table 1. Main oxide composition of FA and LOI (Loss On Ignition)

| Components (wt% as oxides) | | | | | | | | |
|---|---|---|---|---|---|---|---|---|
| $SiO_2$ | $Al_2O_3$ | $Fe_2O_3$ | CaO | MgO | $SO_3$ | $Na_2O$ | $K_2O$ | LOI |
| 49.37 | 29.23 | 2.71 | 6.63 | 1.05 | 0.33 | 0.05 | 0.60 | 3.28 |

613

614

615 Table 2. Mix design of the investigated mortar samples

| Sample | Sand wt% | FA wt% | Cement wt% | 8M NaOH wt% | Na-silicate solution wt% | Water wt% | $Na_2O/SiO_2$ molar ratio [a] | L/B [b] wt/wt ratio | W/B [c] wt/wt ratio |
|---|---|---|---|---|---|---|---|---|---|
| FA12 | 64.00 | 23.70 | - | 1.80 | 8.90 | 1.60 | 0.12 | 0.52 | 0.33 |
| FA14 | 64.00 | 23.70 | - | 3.80 | 6.90 | 1.60 | 0.14 | 0.52 | 0.34 |
| FA16 | 64.00 | 23.70 | - | 5.35 | 5.35 | 1.60 | 0.16 | 0.52 | 0.35 |
| CEM | 64.00 | - | 23.70 | - | - | 12.30 | - | 0.52 | 0.52 |

616 [a] Molar ratio determined by the total content of sodium hydroxide and silica present in the
617 mix, without considering silica content of sand
618 [b] L/B=liquid/binder ratio. L is calculated considering the total content of 8 M NaOH+sodium
619 silicate solution+water
620 [c] W/B=water/binder ratio. W is calculated considering the water contained in the alkaline
621 solutions+the added water

Table 3. Core pH values of the mortar specimens after 1 day curing and after 90 days of partial immersion in 3.5% NaCl solution

| Sample | After 1 d curing | After 90 d of partial immersion in chloride solution |
|---|---|---|
| FA12 | 12.73 | 12.38 |
| FA14 | 12.74 | 12.36 |
| FA16 | 12.73 | 12.17 |
| CEM | 12.99 | 12.88 |

626

627 Table 4. Raman quantitative analysis for corrosion products formed on rebars in reinforced
628 slabs exposed to 3.5% NaCl solution; + = small values detected; ++ = high values detected;
629 Fluor. = fluorescence

| Sample | Akaganeite | Hematite | Maghemite | δ-FeOOH | Fluor. |
|---|---|---|---|---|---|
| FA12 | + | | + | + | ++ |
| FA14 | + | + | + | + | ++ |
| FA16 | + | + | + | + | ++ |
| CEM | | | + | + | ++ |

630

631

Table 5. Elemental analysis (in ppm) of leachate solutions provided by ICP-OES

| Element \ Sample | FA12 | FA14 | FA16 | CEM |
|---|---|---|---|---|
| Si | 540 | 840 | 500 | < 0.5 |
| Al | 0.3 | 1.4 | 0.7 | 1.1 |
| Ca | < 0.1 | < 0.1 | < 0.1 | 60 |
| K | 110 | 130 | 130 | 430 |
| Na | 3900 | 5460 | 5300 | 420 |

Figure(s)

Click here to download high resolution image

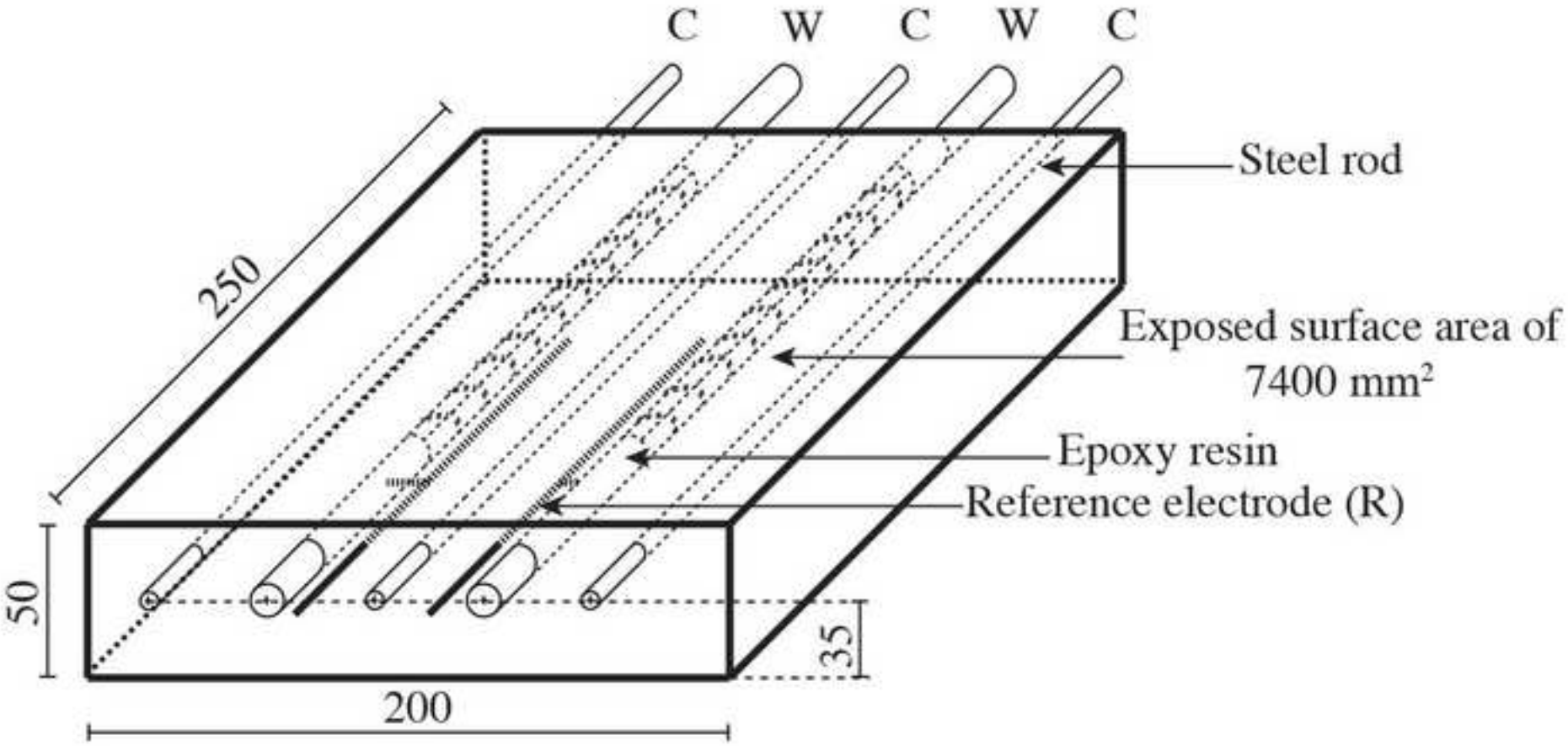

Figure(s)
Click here to download high resolution image

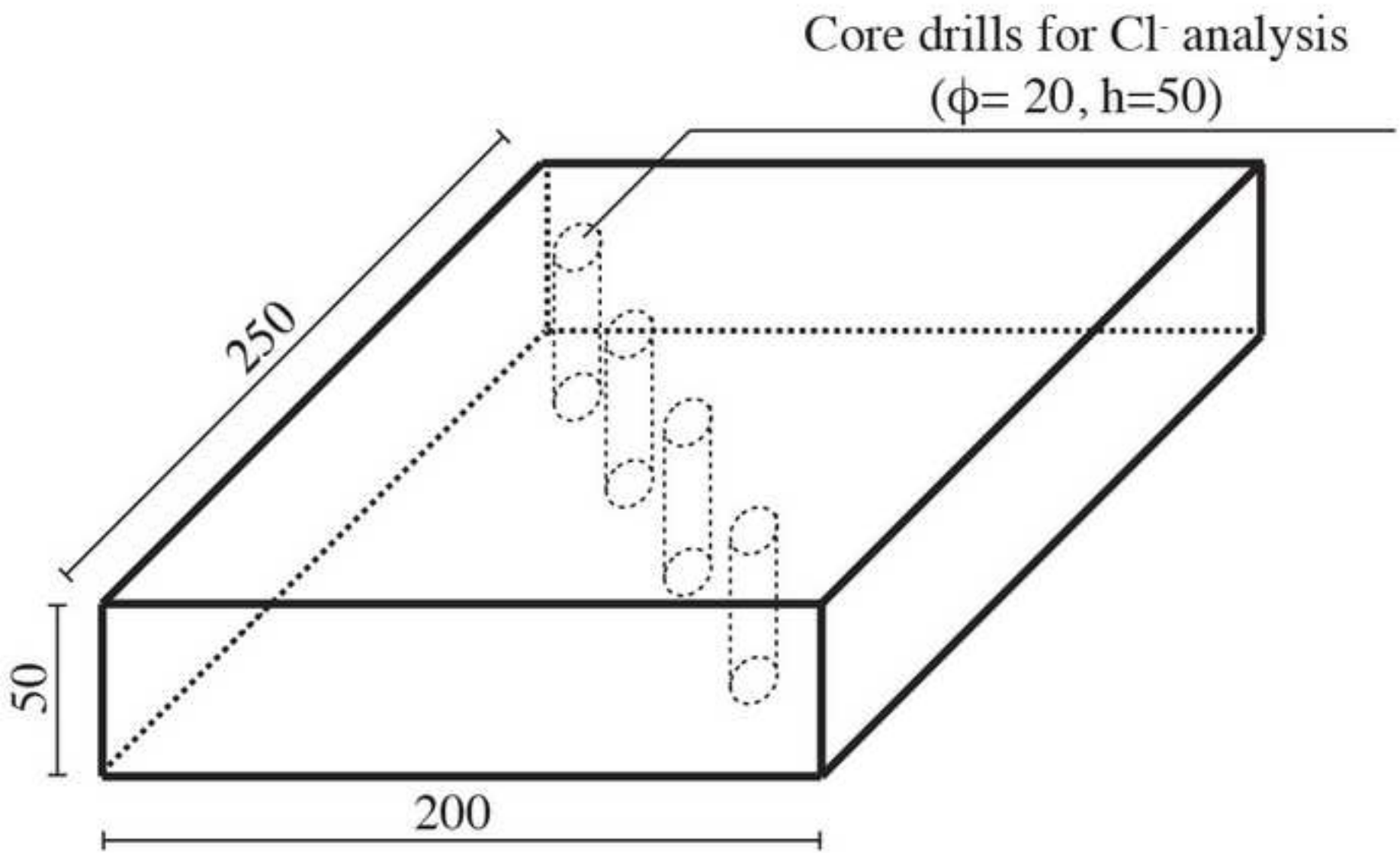

Figure(s)
Click here to download high resolution image

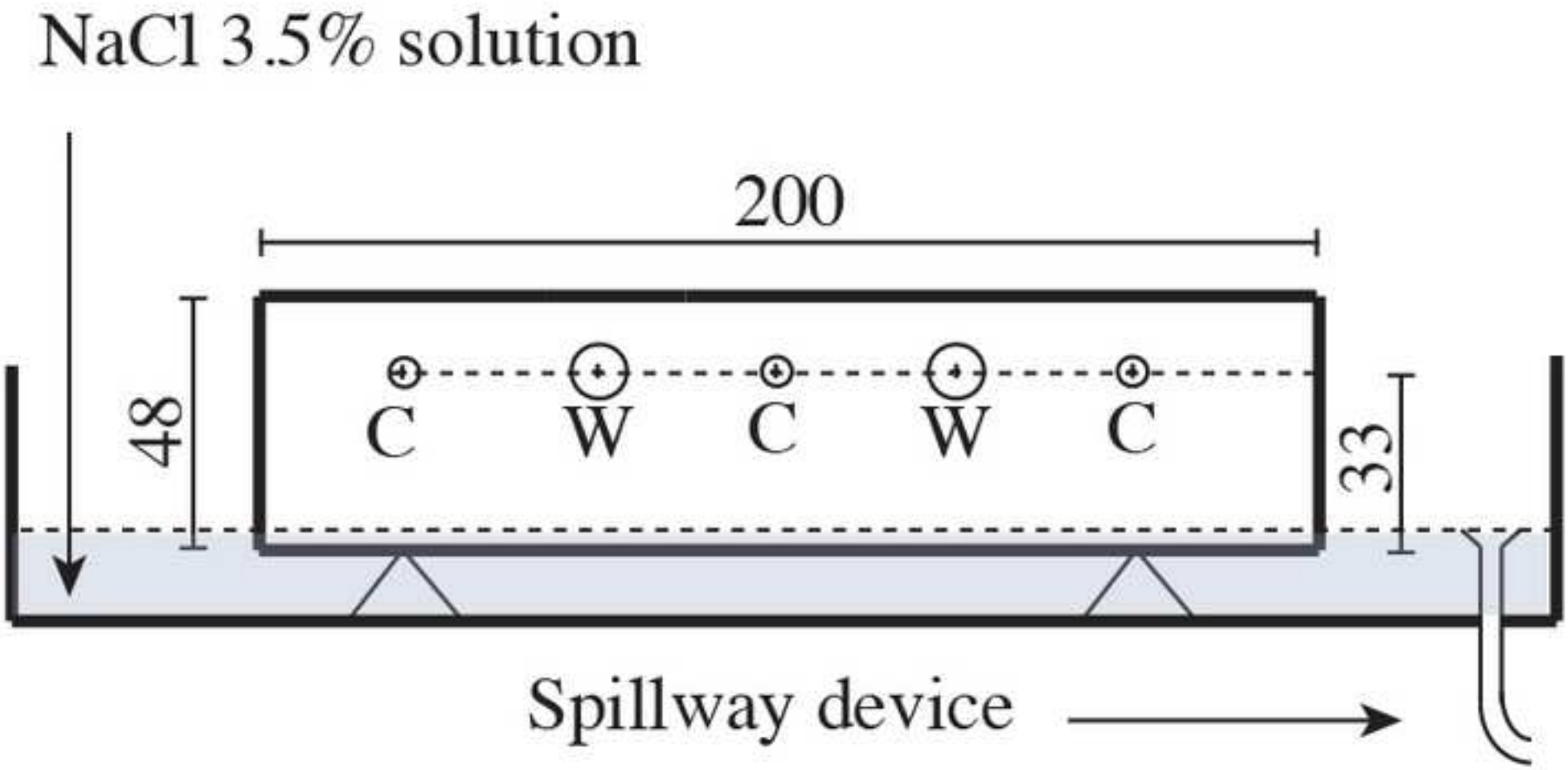

Figure(s)
Click here to download high resolution image

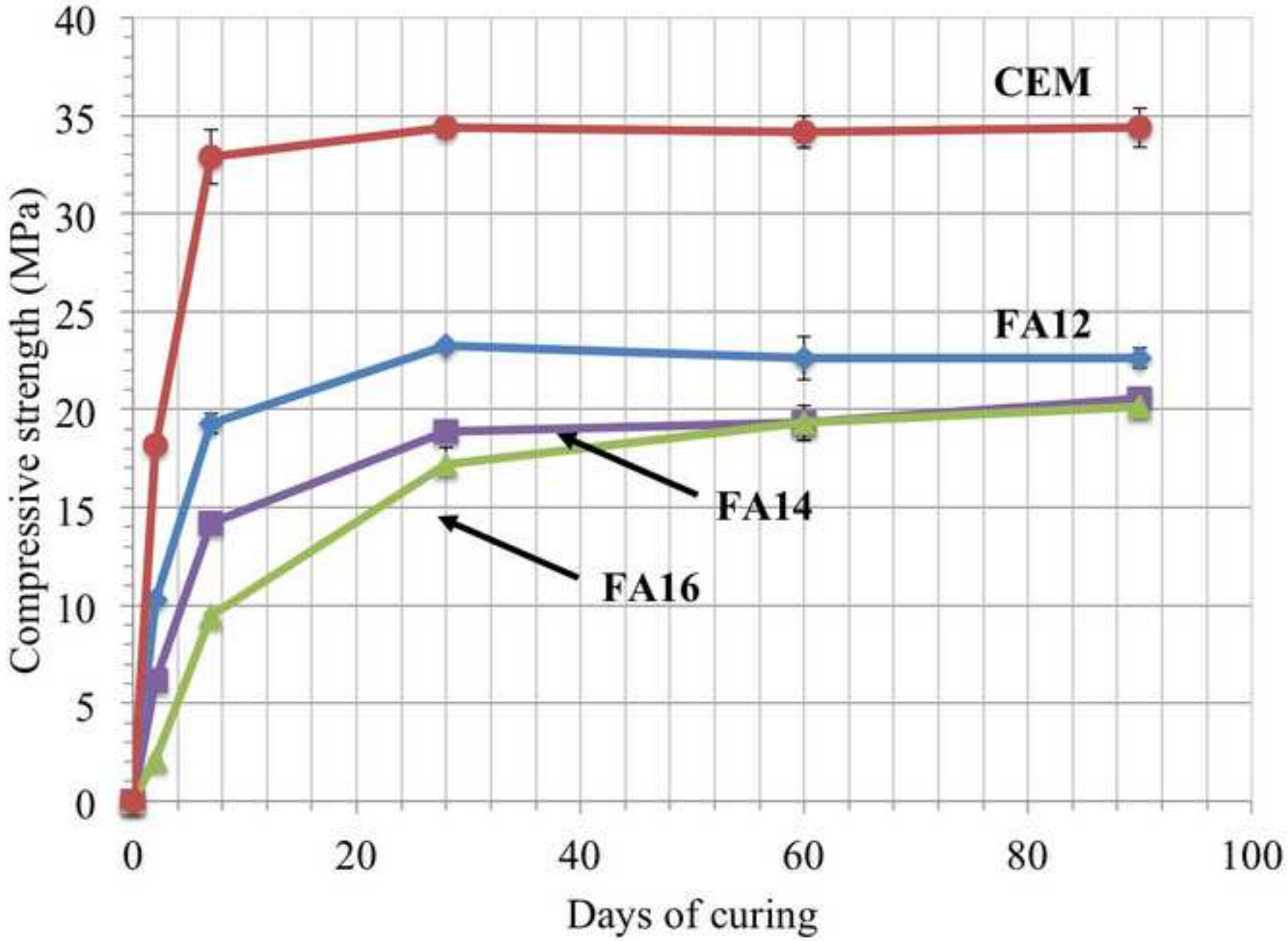

Figure(s)

Click here to download high resolution image

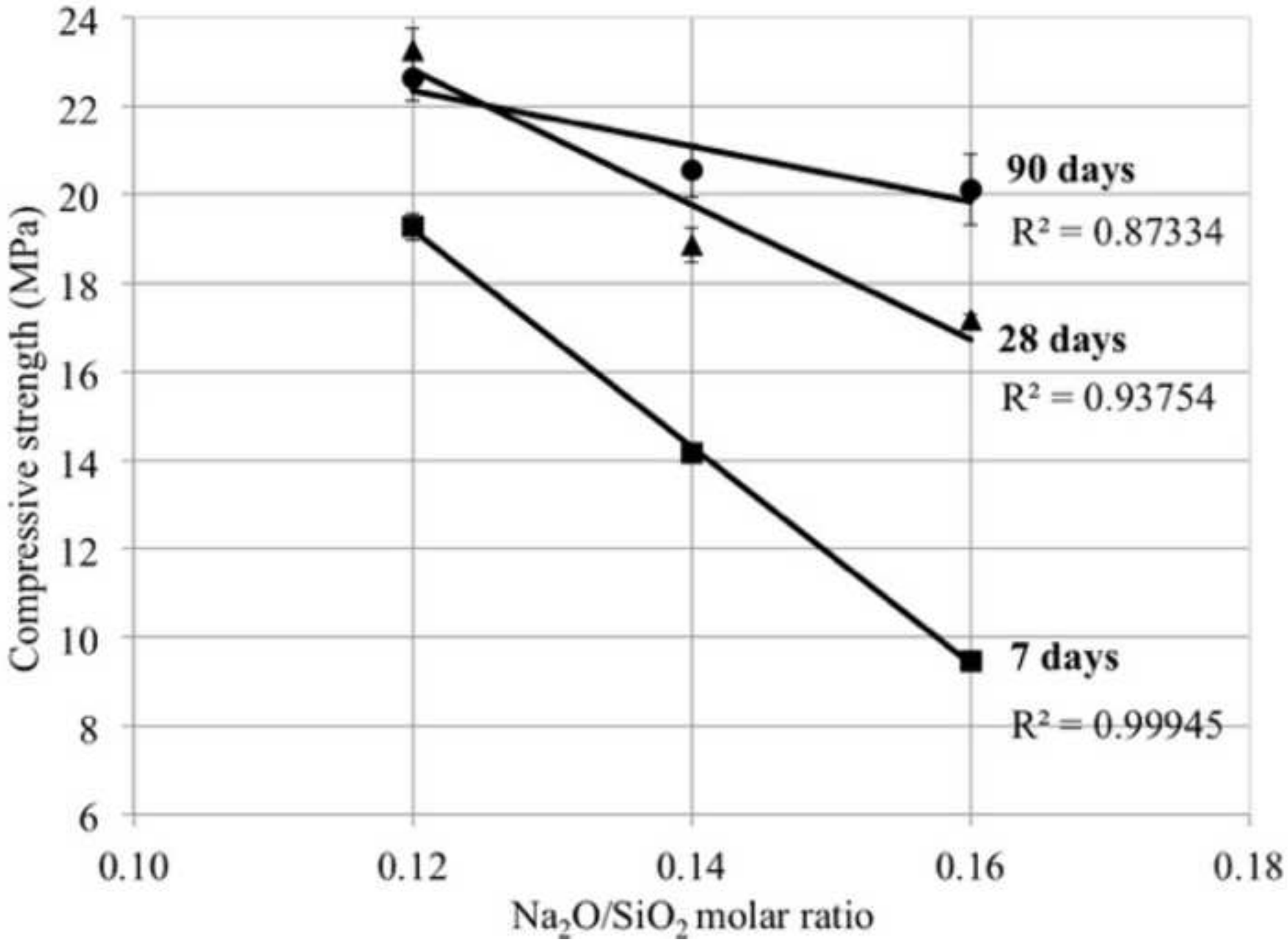

Figure(s)

Click here to download high resolution image

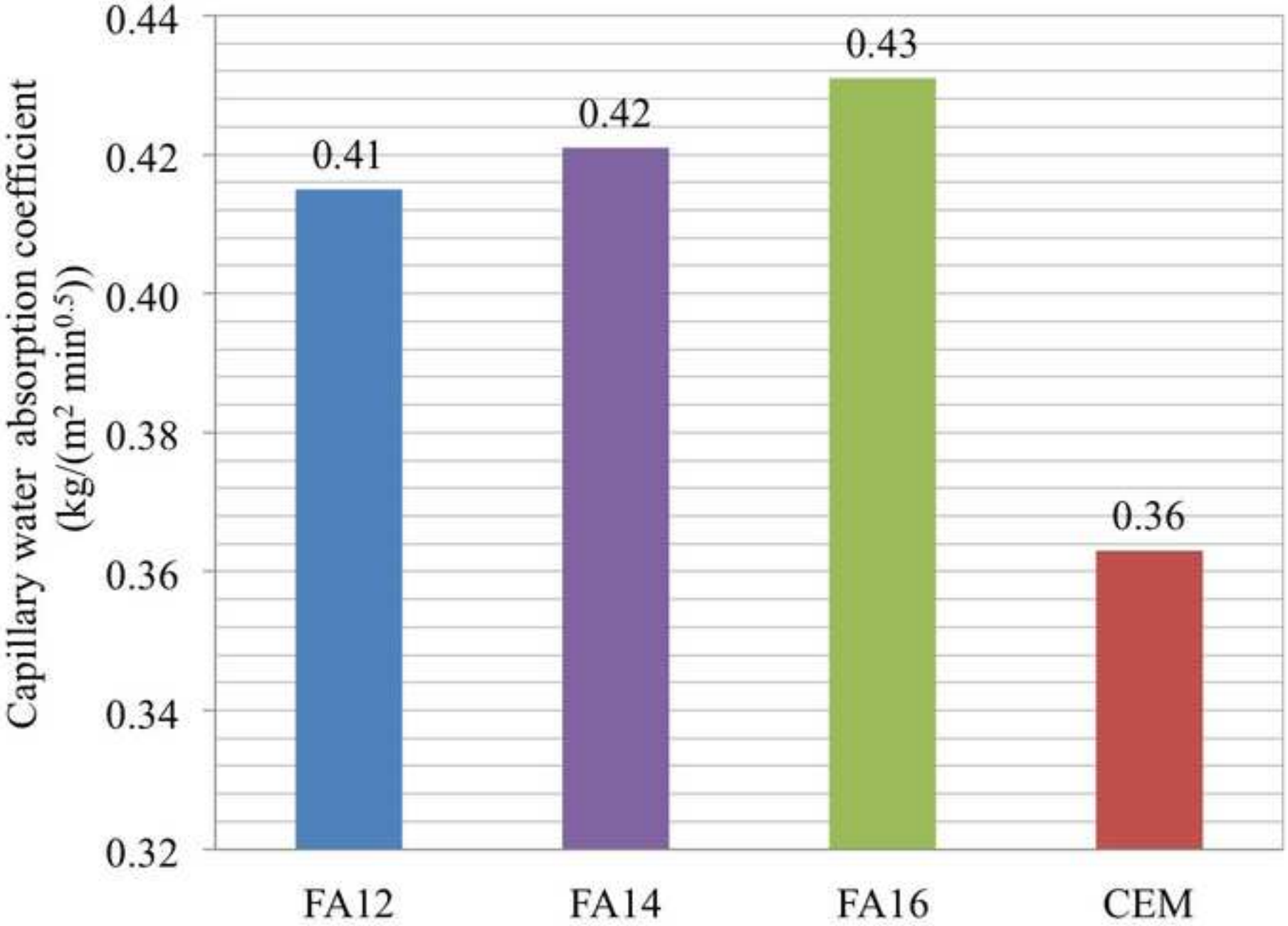

Figure(s)

Click here to download high resolution image

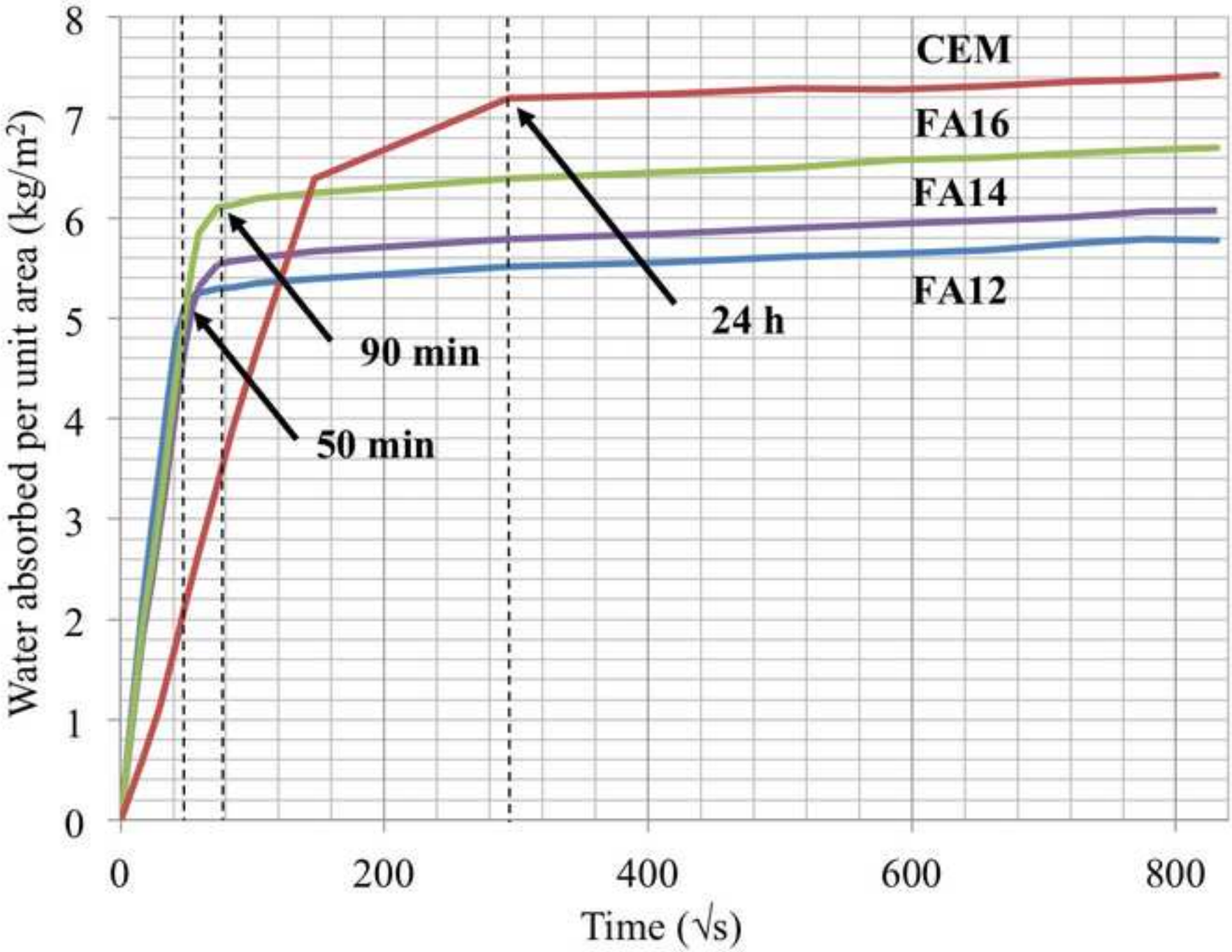

Figure(s)
Click here to download high resolution image

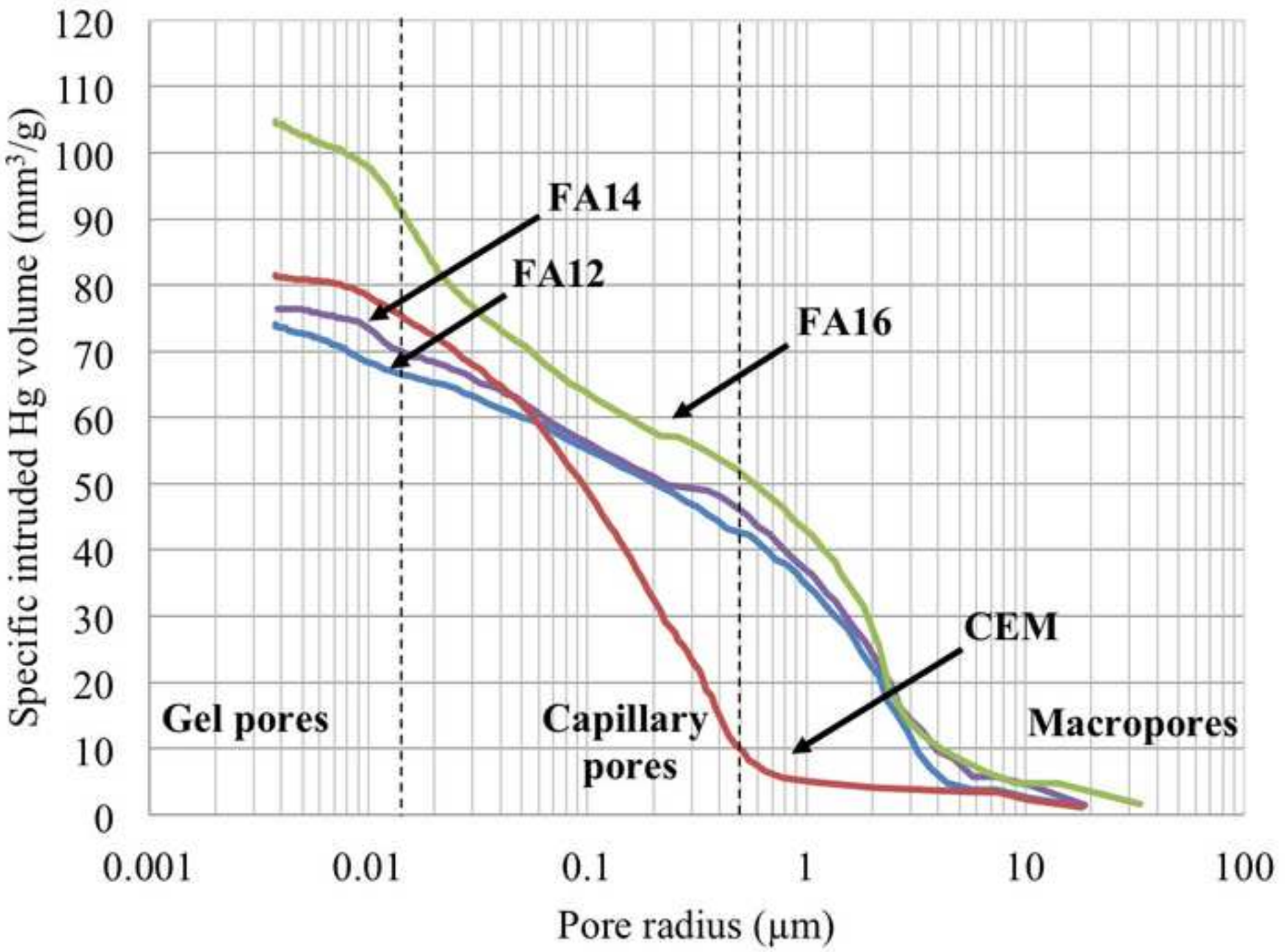

Figure(s)

Click here to download high resolution image

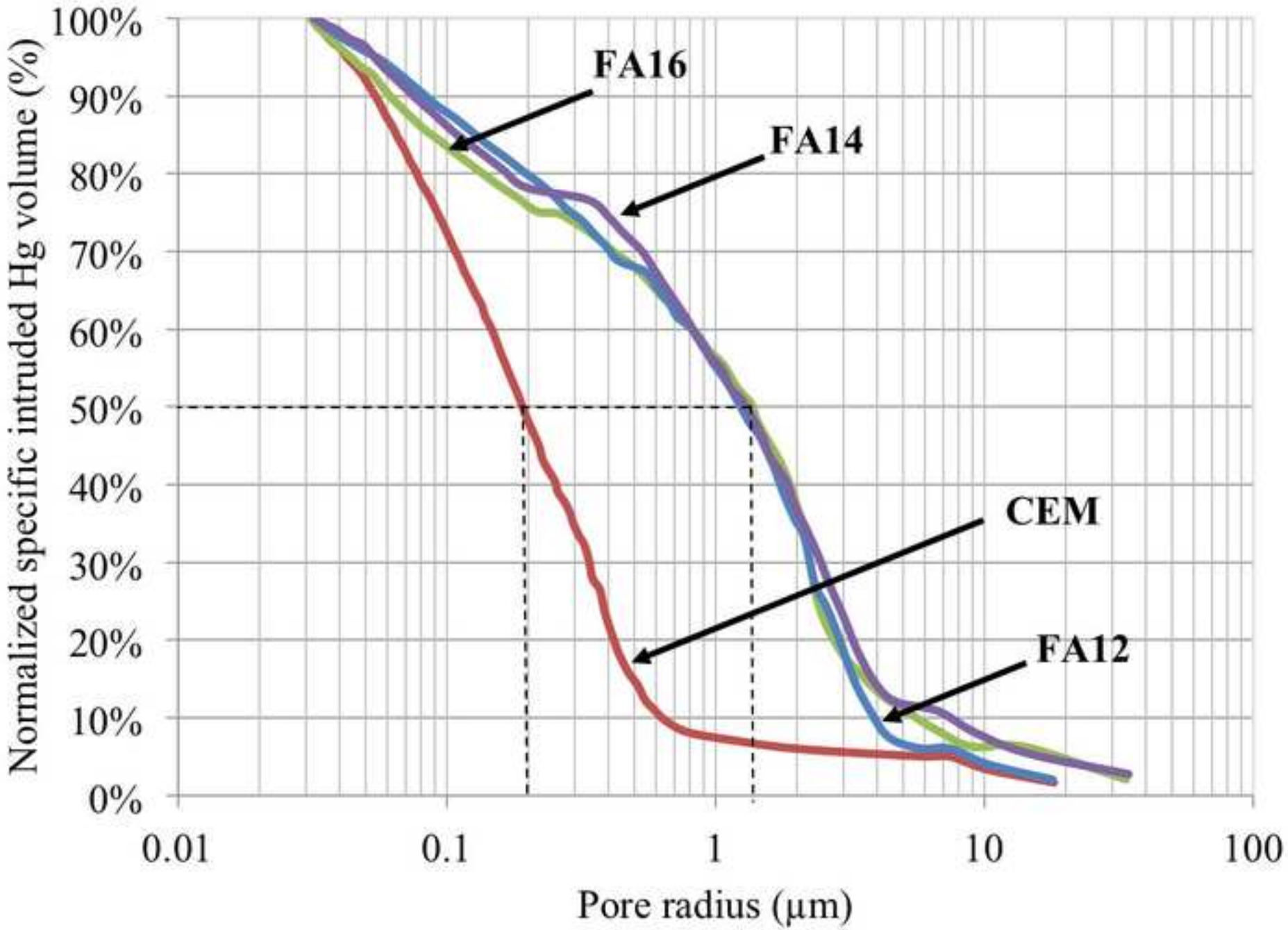

Figure(s)
Click here to download high resolution image

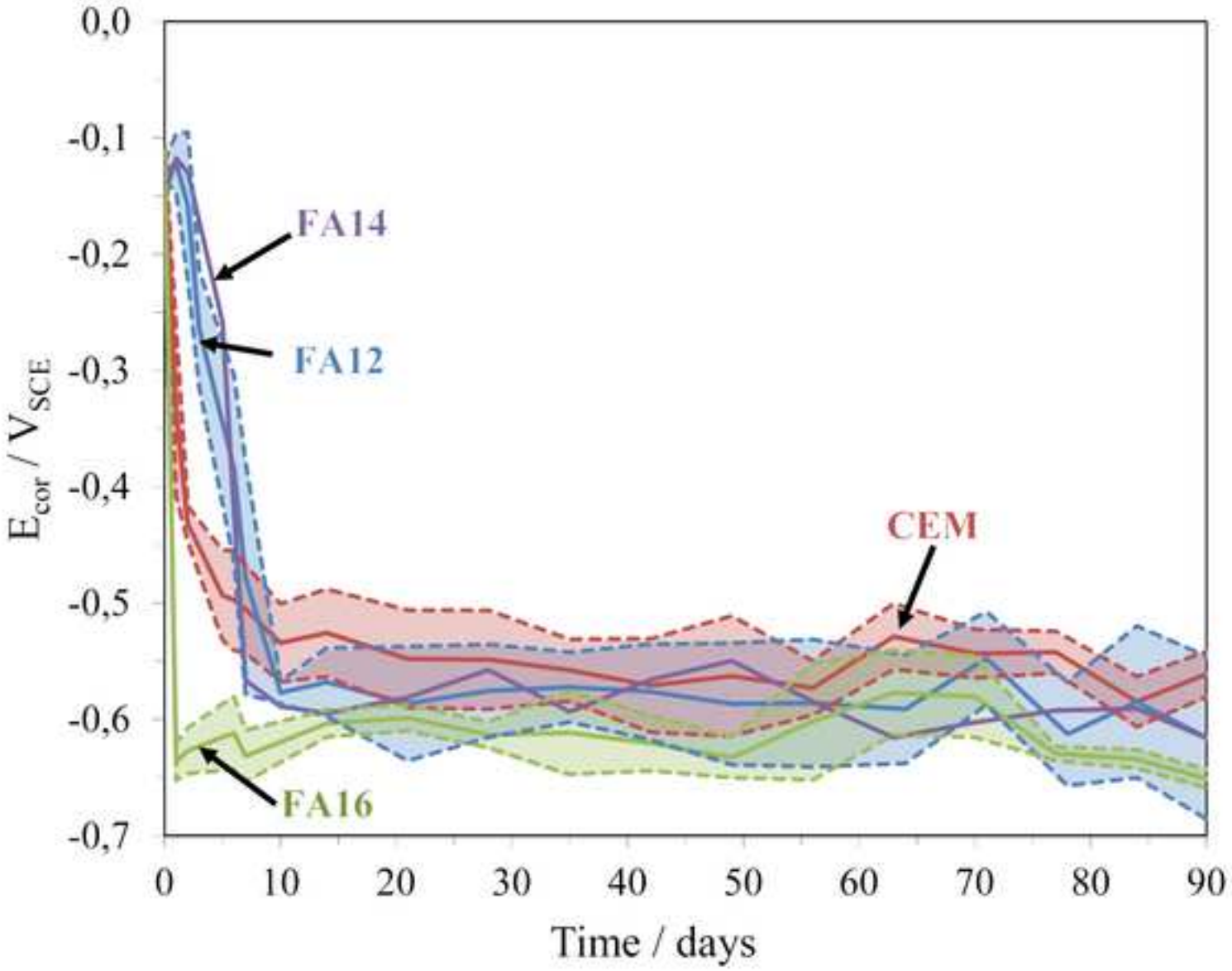

Figure(s)

Click here to download high resolution image

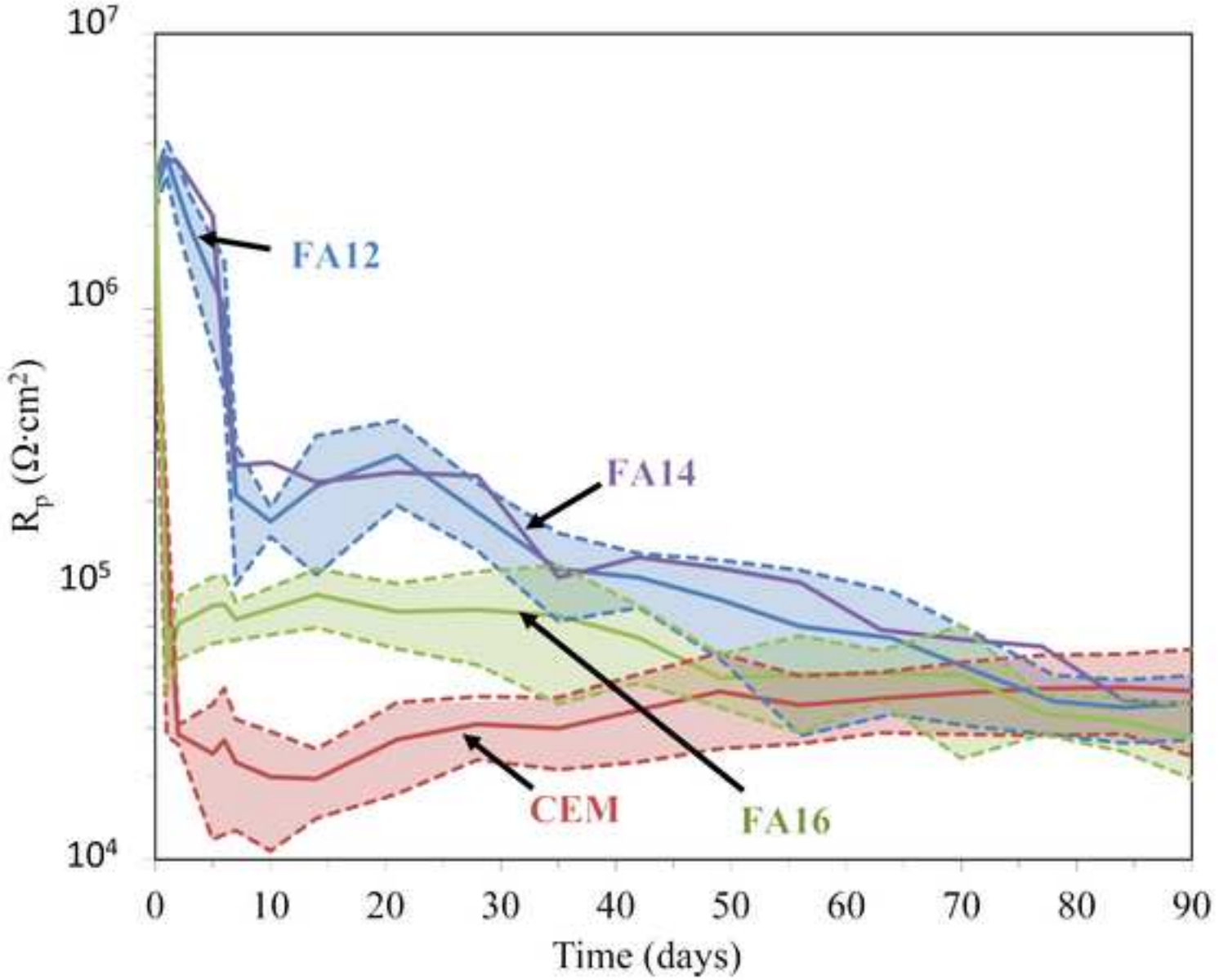

Figure(s)

Click here to download high resolution image

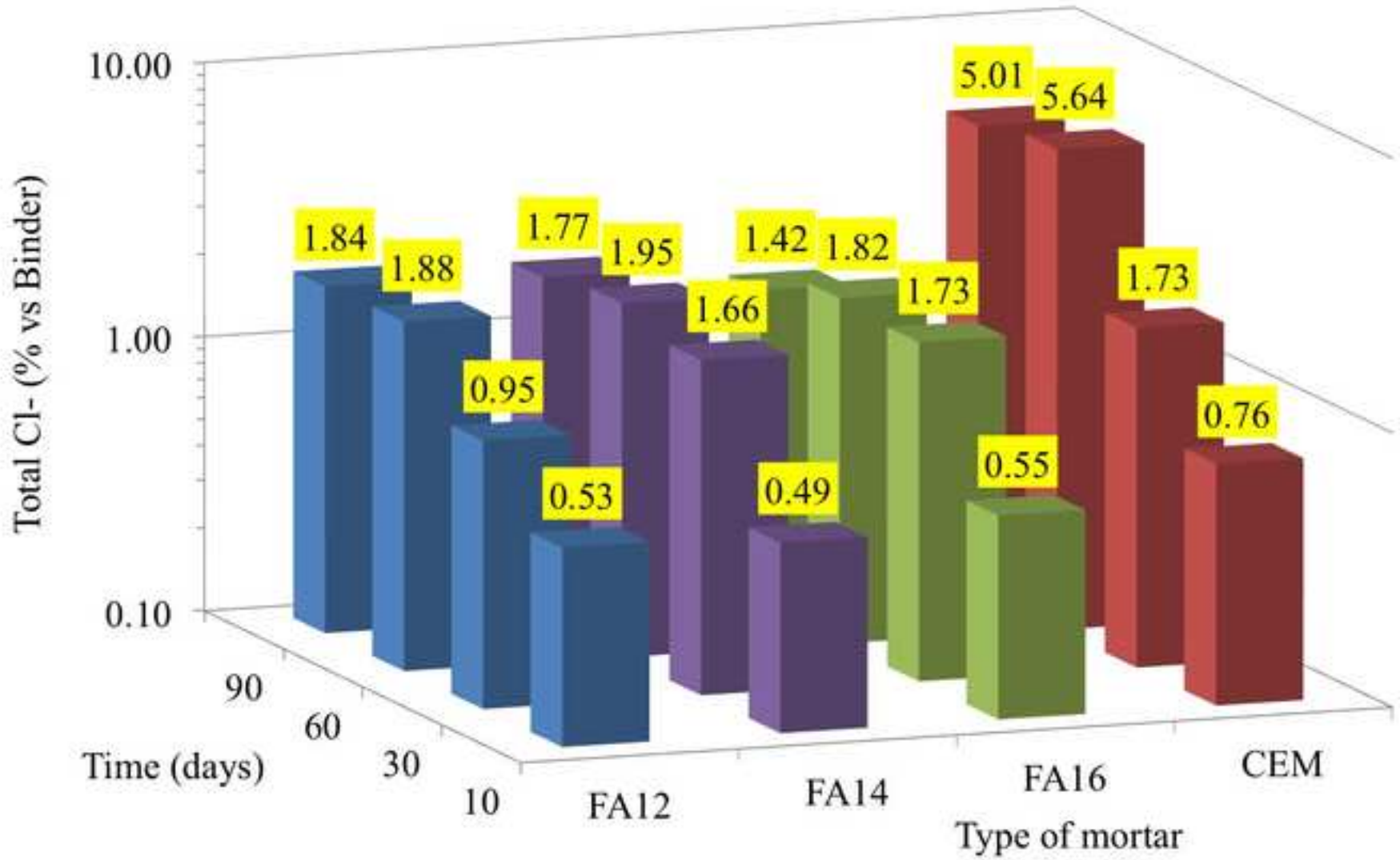

**Figure(s)**

**Click here to download high resolution image**

**Figure(s)**

**Click here to download high resolution image**

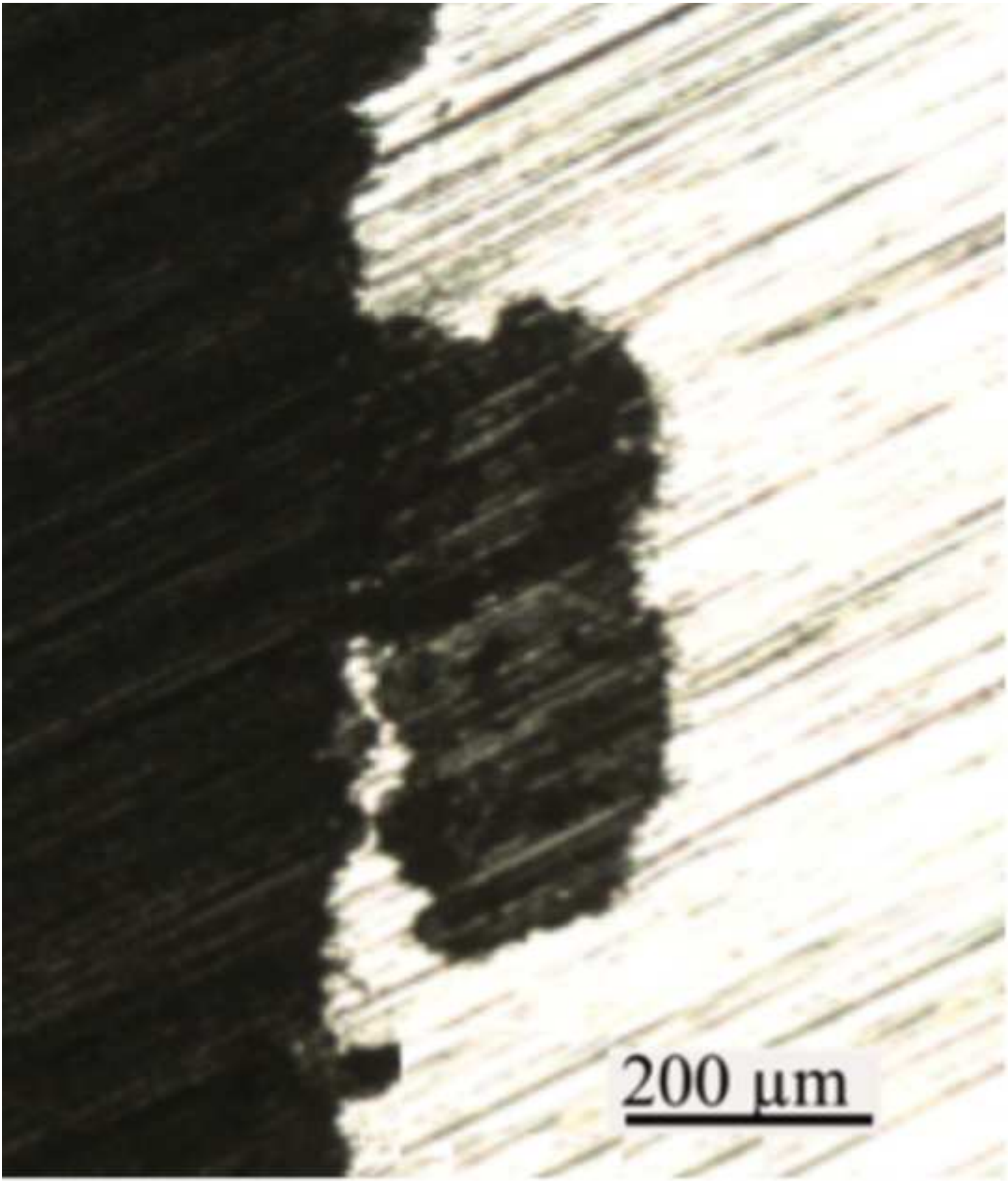

**Figure(s)**

**Click here to download high resolution image**

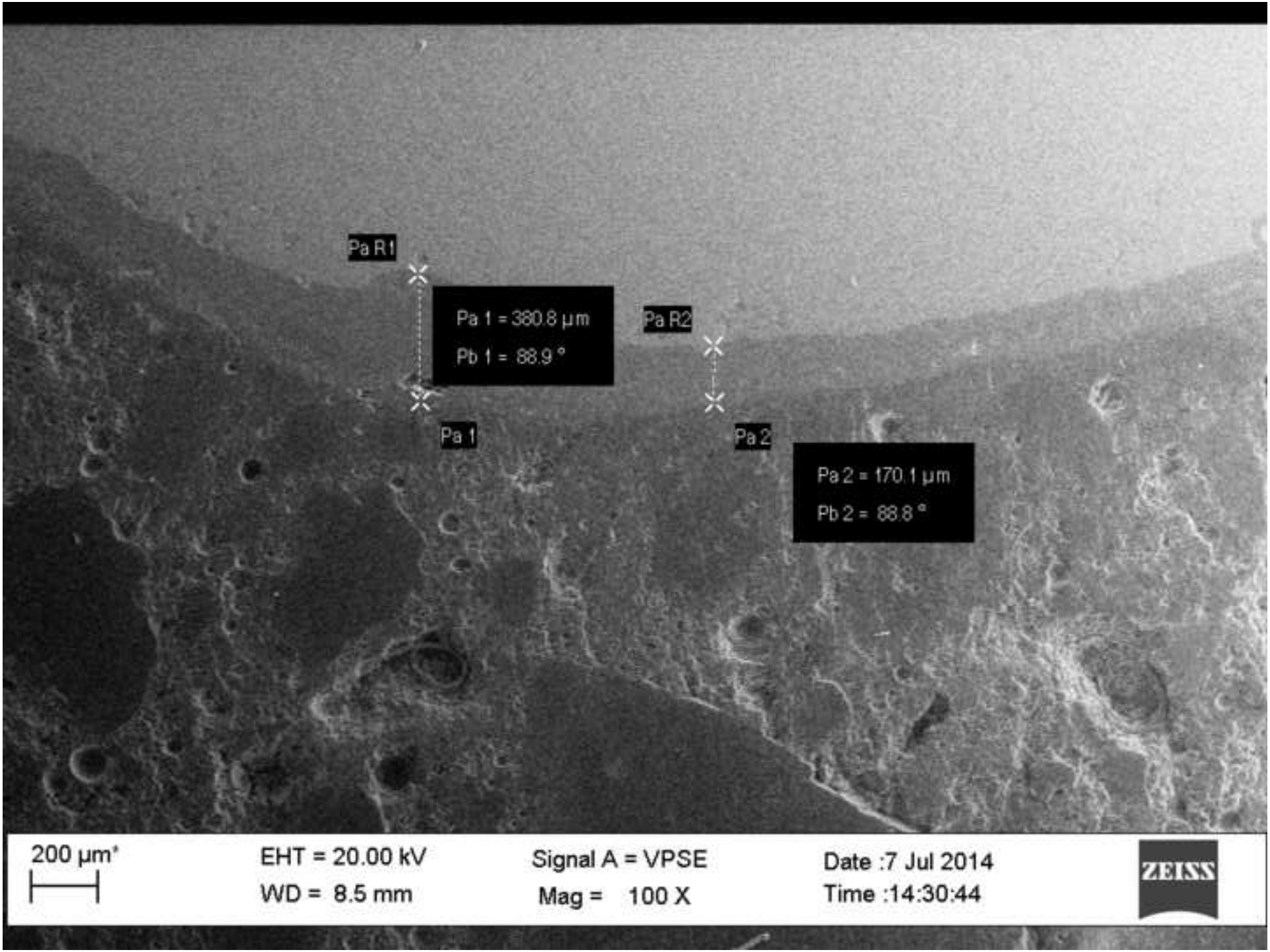

Figure(s)

Click here to download high resolution image